Optimal Hybrid Magnetic Attitude Control: Disturbance Accommodation and Impulse Timing

Behrad Vatankhahghadim and Christopher J. Damaren

***Abstract*— A recently proposed hybrid attitude control scheme, which optimally combines magnetic torques with impulsive thrusting using a continuous/discrete linear quadratic regulator, is modified to accommodate disturbances. Accounting for the presence of disturbances in the design procedure, previous results on necessary conditions for optimality of impulse application times are modified accordingly. In addition, the special case of a multiorbit mission with repeating impulse patterns is considered, showing that an elegant extension of the optimality conditions would significantly reduce the computational cost by limiting the design space to only the first orbit: this extended condition is obtained by summing over all orbits within the control interval, the original conditions being computed at each repeating impulse time. Finally, numerical examples are presented, confirming the superiority of the proposed disturbance-accommodating controller in terms of steady-state performance (even when the disturbance estimates are partly incorrect) and the validity of the extended optimal timing theory in the linear region.**

***Index Terms*— Disturbance accommodation, magnetic attitude control, optimal hybrid control, optimal impulse times.**

I. Introduction

CONTROLLING the attitude of spacecraft is of crucial importance for certain space missions and can be performed via a variety of control schemes and utilizing actuators such as thrusters and magnetic torquers. The latter, which involves making use of the electromagnetic interactions between current-carrying coils and the geomagnetic field, is a particularly attractive option for near-earth spacecraft because of its efficiency and absence of fuel requirements. A survey of the studies performed on magnetic attitude control is provided in [1]. Inherent in this mechanism, however, is the problem of instantaneous underactuation that arises from the resultant torque vector being perpendicular to the magnetic field. In addition, there is an intrinsic gain limitation associated with stabilization using magnetic actuators, as demonstrated in [2], where local stability is shown to be guaranteed only for gains below a certain threshold indicated by a scaling condition.

Owing to the time-varying nature of the magnetic field, the attitude control system of interest possesses, on average, controllability properties (over some time interval) for a range of orbit inclinations [1], [3]. Local and global three-axis stabilization results using purely magnetic control were derived in [4] and [5] relying on the quasi-periodic nature of the earth's magnetic field. Exploiting periodicity, optimal periodic control approaches were proposed in [3], [6], and [7]. Later on, abandoning the periodicity assumption, full-state feedback using only magnetic actuation was proposed for an almost globally stable solution in [8], but the aforementioned scaling condition restricting the control gains remained. Providing an auxiliary impulsive control mechanism to complement the continuous torque of the magnetic controller is, therefore, partly motivated by a desire to alleviate this gain limitation. Such an impulsive/continuous (henceforth called "hybrid") control scheme may also provide improvements in terms of control performance and energy consumption.

Addition of mechanical actuation to work in harmony with magnetic torquers and a geometric technique for decomposing the control vector were considered in [9] and [10], respectively. The combination of magnetic control with impulsive thrusting using linear time-invariant and linear time-periodic approaches was studied in [11]. A hybrid linear quadratic regulator (LQR) that incorporates both types of actuation was proposed in [12], which was in turn based on the results of [13] on optimal hybrid control for spacecraft formation flight. Neither of these references nor those that make use of proportional–derivative magnetic control (such as [2]) or the continuous-only periodic LQR (such as [6]) include the disturbances when designing the control laws. Considering that these disturbances can be estimated (see [18, Sec. 17.2]) and inspired by the disturbance-accommodating (DA) tracking controller suggested in [14], the hybrid attitude controller of [12] is extended to accommodate disturbances.

Optimal periodic disturbance rejection is implemented in [7], but by assuming periodic system and disturbances and compensating for the estimated disturbances using feedforward. The disturbance accommodation approach used in this brief also bears resemblance to that in [15], in which the plant's state and output equations are augmented with some disturbance models and linear quadratic Gaussian is applied to the augmented system; however, this brief also involves discrete dynamics that were not considered in [7] and [15].

In addition to improving the controller proposed in [12] via disturbance rejection, this brief also studies optimal timing of the impulses. Necessary and sufficient conditions were recently developed and validated in [16] for optimality of a set of impulse application times. In this brief, the necessary conditions are modified to reflect the design changes required for disturbance accommodation. In addition, these conditions are extended to apply to multiple orbits, provided that the impulse pattern repeats every orbit. In this special case that allows for

Manuscript received December 21, 2015; revised June 14, 2016; accepted August 21, 2016. Manuscript received in final form August 22, 2016. Recommended by Associate Editor Q. Wang.

The authors are with the Institute for Aerospace Studies, University of Toronto, Toronto, ON M3H 5T6, Canada (e-mail: behrad.vatankhahghadim@mail.utoronto.ca; damaren@utias.utoronto.ca).

Digital Object Identifier 10.1109/TCST.2016.2604739

an elegant extension of the results of [16], the impulse times in the first orbit are treated as design parameters and those in the subsequent orbits are dictated by this selection.

This brief is organized as follows. Section II presents the relationships governing the disturbed attitude motion of a spacecraft with magnetic torquers and thrusters. The model is then linearized in Section III, and the linearization (that includes the disturbances) is used to derive the optimal disturbance-rejecting continuous and impulsive control inputs. Section IV extends the previous optimality conditions to accommodate disturbances and studies (with most of the derivations provided in the Appendix) a special case in which these conditions can be further extended for multiple orbits. Section V presents the simulation results that assess the validity of the extended theory and the performance of the proposed controller. Finally, closing remarks are provided in Section VI.

II. Spacecraft Kinematics and Dynamics

The control torques consist of $\boldsymbol{\tau}_{\text{mag}}$ produced by magnetic torquers and $\boldsymbol{\tau}_{\text{imp}}$ produced by impulsive thrusters, where the latter are represented using Dirac delta functions centered at the $N-1$ impulse times t_k, $k \in \{1, \ldots, N-1\}$. Consistent with [12], only gravity-gradient disturbances $\boldsymbol{\tau}_{\text{gg}}$ and residual magnetic dipoles from on-board electronics $\boldsymbol{\tau}_{\text{md}}$ are considered, because other disturbance sources are assumed to be negligible for near-earth small spacecraft. The rotational dynamics are described by Euler's rigid body equation [17]

$$\begin{aligned}\boldsymbol{\tau} &= \boldsymbol{I}\dot{\boldsymbol{\omega}}_B + \boldsymbol{\omega}_B^{\times}\boldsymbol{I}\boldsymbol{\omega}_B \\ &= \underbrace{\boldsymbol{m}^{\times}\boldsymbol{b}_B}_{\boldsymbol{\tau}_{\text{mag}}} + \underbrace{\sum_{k=1}^{N-1}\boldsymbol{n}_k\delta(t-t_k)}_{\boldsymbol{\tau}_{\text{imp}}} + \underbrace{\frac{3\mu}{|\boldsymbol{r}_B|^5}\boldsymbol{r}_B^{\times}\boldsymbol{I}\boldsymbol{r}_B}_{\boldsymbol{\tau}_{\text{gg}}} + \underbrace{\boldsymbol{m}_{\text{dist}}^{\times}\boldsymbol{b}_B}_{\boldsymbol{\tau}_{\text{md}}} \quad (1)\end{aligned}$$

where $\mu = 3.986 \times 10^{14}$ m^3/s^2 is the earth's gravitational parameter and $\boldsymbol{I}$, $\boldsymbol{\omega}_B$, and $\boldsymbol{r}_B$ are the moment of inertia, and angular velocity, and position vectors expressed in the body-fixed frame, respectively. Magnetic dipole moments and thruster gains are shown by $\boldsymbol{m}$ and $\boldsymbol{n}$, and $\boldsymbol{b}_B$ is the magnetic field vector as expressed in the body frame. The operator $\dot{(\cdot)}$ denotes derivative with respect to time, and the skew-symmetric operator $(\cdot)^{\times}$ acts on any vector $\boldsymbol{v}$ as follows:

$$\boldsymbol{v}^{\times} = \begin{bmatrix} 0 & -v_3 & v_2 \\ v_3 & 0 & -v_1 \\ -v_2 & v_1 & 0 \end{bmatrix}. \quad (2)$$

The body-fixed vector expressions can also be rewritten in terms of their inertial frame representations as $\boldsymbol{b}_B = \boldsymbol{C}_{\text{BG}}\boldsymbol{b}_G$ and $\boldsymbol{r}_B = \boldsymbol{C}_{\text{BG}}\boldsymbol{r}_G$, where $\boldsymbol{C}_{\text{BG}}$ is the rotation matrix from inertial to body-fixed frame and can be computed from the quaternions (representing the attitude), $\boldsymbol{\epsilon} = [\epsilon_1 \ \epsilon_2 \ \epsilon_3]^T$ and η, using $\boldsymbol{C}_{\text{BG}} = (\eta^2 - \boldsymbol{\epsilon}^T\boldsymbol{\epsilon})\boldsymbol{1}_{3\times 3} + 2\boldsymbol{\epsilon}\boldsymbol{\epsilon}^T - 2\eta\boldsymbol{\epsilon}^{\times}$ [17]. It is evident that both disturbances partly depend on attitude. This observation will be used in Section III to separate the attitude-dependent and exogenous portions of the disturbances after linearization. Assuming a Keplerian orbit, the spacecraft's position in the inertial frame $\boldsymbol{r}_G$ is determined and the tilted dipole model of the geomagnetic field (described in [18, Appendix H]) is used to estimate the magnetic field vector $\boldsymbol{b}_G$.

Finally, the rotational kinematics are given by [17]

$$\begin{bmatrix}\dot{\boldsymbol{\epsilon}} \\ \dot{\eta}\end{bmatrix} = \frac{1}{2}\begin{bmatrix}\eta\boldsymbol{1}_{3\times 3} + \boldsymbol{\epsilon}^{\times} \\ -\boldsymbol{\epsilon}^T\end{bmatrix}\boldsymbol{\omega}. \quad (3)$$

The nonlinear differential equations in (1) and (3) fully describe the attitude motion of the spacecraft. Integrating this system of equations numerically over time provides an accurate prediction of the spacecraft's on-orbit attitude.

III. Optimal Disturbance-Accommodating Hybrid Magnetic Attitude Control

Presented in [13] is an optimal hybrid LQR control scheme used for formation flight, which is then applied in [12] to the attitude control problem of interest. The addition of impulsive torques in these references was primarily motivated by a need to overcome pointwise uncontrollability and gain limitations (demonstrated in [2]) of a solely magnetic controller. Inspired by [14], the hybrid magnetic LQR attitude control scheme of [12] is extended to accommodate disturbances. To this end, an additional variable is introduced that acts as a bias term and modifies the states and costates used for adjoining the continuous- and discrete-time dynamics to the cost function. The optimal control laws are then determined using the continuous- and discrete-time Riccati equations, along with a similar set of differential and difference equations for the newly introduced bias, in tandem.

A. Linearized Disturbed Attitude Dynamics

Hybrid LQR requires linearized equations of motion. Adopting Euler angles $\boldsymbol{\theta}$, small angles and rates are assumed such that $\dot{\boldsymbol{\theta}} \approx \boldsymbol{\omega}$ and $\boldsymbol{\theta} \approx 2\boldsymbol{\epsilon}$. As noted earlier, the disturbances in (1) are partly dependent on the attitude. We have

$$\boldsymbol{\tau}_{\text{md}} = \boldsymbol{m}_{\text{dist}}^{\times}\boldsymbol{b}_B = \boldsymbol{m}_{\text{dist}}^{\times}(\boldsymbol{C}_{\text{BG}}\boldsymbol{b}_G) \quad (4a)$$

$$\boldsymbol{\tau}_{\text{gg}} = \frac{3\mu}{|\boldsymbol{r}_B|^5}\boldsymbol{r}_B^{\times}\boldsymbol{I}\boldsymbol{r}_B \approx \frac{3\mu}{|\boldsymbol{r}_G|^5}(\boldsymbol{C}_{\text{BG}}\boldsymbol{r}_G)^{\times}\boldsymbol{I}(\boldsymbol{C}_{\text{BG}}\boldsymbol{r}_G). \quad (4b)$$

With small angles, $\boldsymbol{C}_{\text{BG}} \approx \boldsymbol{1} - \boldsymbol{\theta}^{\times}$, where $\boldsymbol{1}$ is the identity matrix. Substituting this into (4), using skew symmetry of $(\cdot)^{\times}$, and neglecting second-order terms with $\boldsymbol{\theta}^{\times}\boldsymbol{\theta}^{\times}$, we have

$$\boldsymbol{\tau}_{\text{md}} \approx \boldsymbol{m}_{\text{dist}}^{\times}\boldsymbol{b}_G + \boldsymbol{m}_{\text{dist}}^{\times}\boldsymbol{b}_G^{\times}\boldsymbol{\theta} \quad (5a)$$

$$\boldsymbol{\tau}_{\text{gg}} \approx \frac{3\mu}{|\boldsymbol{r}_G|^5}\left[\boldsymbol{r}_G^{\times}\boldsymbol{I}\boldsymbol{r}_G + \left(\boldsymbol{r}_G^{\times}\boldsymbol{I}\boldsymbol{r}_G^{\times} - (\boldsymbol{I}\boldsymbol{r}_G)^{\times}\boldsymbol{r}_G^{\times}\right)\boldsymbol{\theta}\right]. \quad (5b)$$

The linearization of (1) and (3) is then provided by

$$\underbrace{\begin{bmatrix}\dot{\boldsymbol{\theta}} \\ \ddot{\boldsymbol{\theta}}\end{bmatrix}}_{\dot{\boldsymbol{x}}(t)} \approx \underbrace{\begin{bmatrix}\boldsymbol{0} & \boldsymbol{1} \\ \boldsymbol{\alpha} & \boldsymbol{0}\end{bmatrix}}_{\boldsymbol{A}_c(t)}\underbrace{\begin{bmatrix}\boldsymbol{\theta} \\ \dot{\boldsymbol{\theta}}\end{bmatrix}}_{\boldsymbol{x}(t)} + \underbrace{\begin{bmatrix}\boldsymbol{0} \\ -\boldsymbol{I}^{-1}\boldsymbol{b}_G^{\times}\end{bmatrix}}_{\boldsymbol{B}_c(t)}\underbrace{[\boldsymbol{m}]}_{\boldsymbol{u}(t)} + \underbrace{\begin{bmatrix}\boldsymbol{0} \\ \boldsymbol{\beta}\end{bmatrix}}_{\boldsymbol{d}(t)}, \ t \neq t_k \quad (6a)$$

$$\underbrace{\begin{bmatrix}\boldsymbol{\theta}_k^+ \\ \dot{\boldsymbol{\theta}}_k^+\end{bmatrix}}_{\boldsymbol{x}(t_k^+)} \approx \underbrace{\begin{bmatrix}\boldsymbol{1} & \boldsymbol{0} \\ \boldsymbol{0} & \boldsymbol{1}\end{bmatrix}}_{\boldsymbol{A}_{dk}}\underbrace{\begin{bmatrix}\boldsymbol{\theta}_k^- \\ \dot{\boldsymbol{\theta}}_k^-\end{bmatrix}}_{\boldsymbol{x}(t_k^-)} + \underbrace{\begin{bmatrix}\boldsymbol{0} \\ \boldsymbol{I}^{-1}\end{bmatrix}}_{\boldsymbol{B}_{dk}}\underbrace{[\boldsymbol{n}_k]}_{\boldsymbol{v}_k}, \quad t = t_k \quad (6b)$$

where $\boldsymbol{\theta}_k^{\pm} \triangleq \boldsymbol{\theta}(t_k^{\pm})$. The correction term $\boldsymbol{\alpha}$ is given by $\boldsymbol{\alpha}(t) = \boldsymbol{I}^{-1}[\boldsymbol{m}_{\text{dist}}^{\times}\boldsymbol{b}_G^{\times} + (3\mu/|\boldsymbol{r}_G|^5)(\boldsymbol{r}_G^{\times}\boldsymbol{I}\boldsymbol{r}_G^{\times} - (\boldsymbol{I}\boldsymbol{r}_G)^{\times}\boldsymbol{r}_G^{\times})]$ and modifies $\boldsymbol{A}_c(t)$ to account for the attitude-dependent portion of the disturbance torques. The vector $\boldsymbol{x}(t)$ is the state, the vectors $\boldsymbol{u}(t)$ and $\boldsymbol{v}_k$ are the continuous and impulsive control inputs, respectively, and $\boldsymbol{d}(t)$ contains the exogenous disturbances, with $\boldsymbol{\beta}(t) = \boldsymbol{I}^{-1}[\boldsymbol{m}_{\text{dist}}^{\times}\boldsymbol{b}_G + (3\mu/|\boldsymbol{r}_G|^5)(\boldsymbol{r}_G^{\times}\boldsymbol{I}\boldsymbol{r}_G)]$. There are $N-1$ impulses applied at t_k, $k \in \{1, 2, \ldots, N-1\}$, and t_k^- and t_k^+ are the instants right before and right after an impulse, respectively. A small $\boldsymbol{m}$ is assumed.

B. Design of the Disturbance-Accommodating Hybrid LQR

Consistent with [12] and [13], the performance index is

$$J \triangleq \frac{1}{2}\sum_{k=0}^{N-1}\int_{t_k^+}^{t_{k+1}^-}[\boldsymbol{x}^T(t)\boldsymbol{Q}_c(t)\boldsymbol{x}(t) + \boldsymbol{u}^T(t)\boldsymbol{R}_c(t)\boldsymbol{u}(t)]dt + \frac{1}{2}\sum_{k=1}^{N-1}\left[\boldsymbol{x}_k^{-T}\boldsymbol{Q}_{dk}\boldsymbol{x}_k^- + \boldsymbol{v}_k^T\boldsymbol{R}_{dk}\boldsymbol{v}_k\right] + \frac{1}{2}\boldsymbol{x}_f^T\boldsymbol{S}\boldsymbol{x}_f \quad (7)$$

where $\boldsymbol{x}_k^- \triangleq \boldsymbol{x}(t_k^-)$ and $\boldsymbol{x}_f \triangleq \boldsymbol{x}(t_f)$, with t_f denoting the end time. In addition, $t_0^+ \triangleq t_0$ and $t_N^- \triangleq t_f$, and $\boldsymbol{S} = \boldsymbol{S}^T \geqslant 0$ sets the terminal state penalty. The matrices $\boldsymbol{Q}_c(t) = \boldsymbol{Q}_c^T(t) \geqslant 0$ and $\boldsymbol{R}_c(t) = \boldsymbol{R}_c^T(t) > 0$ set the continuous-time state and control penalties and $\boldsymbol{Q}_{dk} = \boldsymbol{Q}_{dk}^T \geqslant 0$ and $\boldsymbol{R}_{dk} = \boldsymbol{R}_{dk}^T > 0$ set the discrete-time state and control penalties, respectively.

The continuous and discrete Hamiltonians are defined as

$$\mathscr{H}_c(t) \triangleq \frac{1}{2}\boldsymbol{x}^T(t)\boldsymbol{Q}_c(t)\boldsymbol{x}(t) + \frac{1}{2}\boldsymbol{u}^T(t)\boldsymbol{R}_c(t)\boldsymbol{u}(t) + \boldsymbol{\lambda}^T(t)(\boldsymbol{A}_c(t)\boldsymbol{x}(t) + \boldsymbol{B}_c(t)\boldsymbol{u}(t) + \boldsymbol{d}(t)) \quad (8a)$$

$$\mathscr{H}_d(t_k) \triangleq \frac{1}{2}\boldsymbol{x}^T(t_k^-)\boldsymbol{Q}_{dk}\boldsymbol{x}(t_k^-) + \frac{1}{2}\boldsymbol{v}_k^T\boldsymbol{R}_{dk}\boldsymbol{v}_k + \boldsymbol{v}_k^T(\boldsymbol{A}_{dk}\boldsymbol{x}(t_k^-) + \boldsymbol{B}_{dk}\boldsymbol{v}_k). \quad (8b)$$

Rewriting (7) using (8), taking the first variation δJ with respect to $\boldsymbol{x}(t)$, $\boldsymbol{x}(t_k^+)$, $\boldsymbol{u}(t)$, and $\boldsymbol{v}_k$, and setting $\delta J = 0$ yield the same conditions at those in [13]

$$\boldsymbol{\lambda}(t_f) = \boldsymbol{S}\boldsymbol{x}(t_f) \quad (9a)$$

$$\dot{\boldsymbol{\lambda}}(t) = -\boldsymbol{Q}_c(t)\boldsymbol{x}(t) - \boldsymbol{A}_c^T(t)\boldsymbol{\lambda}(t) \quad (9b)$$

$$\boldsymbol{\lambda}(t_k^-) = \boldsymbol{Q}_{dk}\boldsymbol{x}(t_k^-) + \boldsymbol{A}_{dk}^T\boldsymbol{v}_k \quad (9c)$$

$$\boldsymbol{\lambda}(t_k^+) = \boldsymbol{v}_k \quad (9d)$$

$$\boldsymbol{u}^*(t) = -\boldsymbol{R}_c^{-1}(t)\boldsymbol{B}_c^T(t)\boldsymbol{\lambda}(t) \quad (9e)$$

$$\boldsymbol{v}_k^* = -\boldsymbol{R}_{dk}^{-1}\boldsymbol{B}_{dk}^T\boldsymbol{v}_k \quad (9f)$$

where (9a) and (9b) describe the evolution of and terminal condition for the continuous costates $\boldsymbol{\lambda}$, (9c) induces a discontinuity in $\boldsymbol{\lambda}$ at each impulse, (9d) relates the continuous costates to the discrete ones $\boldsymbol{v}$, and (9e) and (9f) yield the optimal continuous and impulsive control inputs, respectively.

From (6a) and (9e), the closed-loop continuous-time dynamics for $\dot{\boldsymbol{x}}$ are obtained, which, together with (9b), give

$$\begin{bmatrix}\dot{\boldsymbol{x}}\\ \dot{\boldsymbol{\lambda}}\end{bmatrix} = \begin{bmatrix}\boldsymbol{A}_c & -\boldsymbol{B}_c\boldsymbol{R}_c^{-1}\boldsymbol{B}_c^T\\ -\boldsymbol{Q}_c & -\boldsymbol{A}_c^T\end{bmatrix}\begin{bmatrix}\boldsymbol{x}\\ \boldsymbol{\lambda}\end{bmatrix} + \begin{bmatrix}\boldsymbol{d}\\ \boldsymbol{0}\end{bmatrix}. \quad (10)$$

Following a similar approach as that of [19, Sec. 9-3] (disregarding disturbances, with extension of the results on p. 804), it can be shown that $\boldsymbol{\lambda}(t) = \boldsymbol{P}(t)\boldsymbol{x}(t) + \boldsymbol{h}(t)$ is an appropriate form for the solution. Substituting the biased linear form of $\boldsymbol{\lambda}$ into (9b) and rearranging, using part of (10), yield

$$(\dot{\boldsymbol{P}} + \boldsymbol{P}\boldsymbol{A}_c - \boldsymbol{P}\boldsymbol{B}_c\boldsymbol{R}_c^{-1}\boldsymbol{B}_c^T\boldsymbol{P} + \boldsymbol{Q}_c + \boldsymbol{A}_c^T\boldsymbol{P})\boldsymbol{x} = -\dot{\boldsymbol{h}} + (\boldsymbol{P}\boldsymbol{B}_c\boldsymbol{R}_c^{-1}\boldsymbol{B}_c^T - \boldsymbol{A}_c^T)\boldsymbol{h} - \boldsymbol{P}\boldsymbol{d}. \quad (11)$$

Since (11) must hold for all $\boldsymbol{x}(t)$, both sides should be zero. Similarly, since $\boldsymbol{\lambda}(t_f) = \boldsymbol{P}(t_f)\boldsymbol{x}(t_f) + \boldsymbol{h}(t_f) = \boldsymbol{S}\boldsymbol{x}(t_f)$ from (9a), we should also have $(\boldsymbol{P}(t_f) - \boldsymbol{S})\boldsymbol{x}(t_f) = -\boldsymbol{h}(t_f) = \boldsymbol{0}$, each of which yields a terminal condition for one of the following differential equations (assuming arbitrary states at the end time), for the last time interval, $t \in (t_{n-1}, t_f)$:

$$\dot{\boldsymbol{P}}(t) = -\big[\boldsymbol{Q}_c(t) + \boldsymbol{P}(t)\boldsymbol{A}_c(t) + \boldsymbol{A}_c^T(t)\boldsymbol{P}(t) - \boldsymbol{P}(t)\boldsymbol{B}_c(t)\boldsymbol{R}_c^{-1}\boldsymbol{B}_c^T(t)\boldsymbol{P}(t)\big], \quad \boldsymbol{P}(t_f) = \boldsymbol{S} \quad (12a)$$

$$\dot{\boldsymbol{h}}(t) = -\big[\boldsymbol{A}_c(t) - \boldsymbol{B}_c(t)\boldsymbol{R}_c^{-1}(t)\boldsymbol{B}_c^T(t)\boldsymbol{P}(t)\big]^T\boldsymbol{h}(t) - \boldsymbol{P}(t)\boldsymbol{d}(t), \quad \boldsymbol{h}(t_f) = \boldsymbol{0} \quad (12b)$$

which can be integrated backward simultaneously. This result is consistent with that of [14, eqs. (8) and (9)] and [19, eq. (9-287)], from which the tracking portion is eliminated. Once an impulse is reached, however, there will be discontinuities in $\boldsymbol{x}(t)$ owing to the discrete dynamics, hence requiring difference equations for $\boldsymbol{P}$ and $\boldsymbol{h}$ at each impulse.

From (6b), (9f), and (9d), the closed-loop discrete dynamics are obtained for $\boldsymbol{x}(t_k^+)$, rearranging which for $\boldsymbol{x}(t_k^-)$ and using $\boldsymbol{x}(t_k^+) = \boldsymbol{P}^{-1}(t_k^+)[\boldsymbol{\lambda}(t_k^+) - \boldsymbol{h}(t_k^+)]$ after an impulse yield

$$\boldsymbol{x}(t_k^-) = \boldsymbol{A}_{dk}^{-1}(\boldsymbol{P}^{-1}(t_k^+) + \boldsymbol{B}_{dk}\boldsymbol{R}_{dk}^{-1}\boldsymbol{B}_{dk}^T)\boldsymbol{\lambda}(t_k^+) - \boldsymbol{A}_{dk}^{-1}\boldsymbol{P}^{-1}(t_k^+)\boldsymbol{h}(t_k^+) \quad (13)$$

in which the preimpulse states are given in terms of the postimpulse variables, which will be known while integrating backward. Furthermore, from (9c) and (9d)

$$\boldsymbol{\lambda}(t_k^-) = \boldsymbol{Q}_{dk}\boldsymbol{x}(t_k^-) + \boldsymbol{A}_{dk}^T\boldsymbol{\lambda}(t_k^+) \quad (14)$$

in which (13) can be substituted, and once the result is rearranged, together with (13), it gives the following closed-loop discrete system that is analogous to the continuous one in (10):

$$\begin{bmatrix}\boldsymbol{x}(t_k^-)\\ \boldsymbol{\lambda}(t_k^-)\end{bmatrix} = \begin{bmatrix}\boldsymbol{0} & \boldsymbol{A}_{dk}^{-1}\boldsymbol{Z}_k\\ \boldsymbol{0} & \boldsymbol{Q}_{dk}\boldsymbol{A}_{dk}^{-1}\boldsymbol{Z}_k + \boldsymbol{A}_{dk}^T\end{bmatrix}\begin{bmatrix}\boldsymbol{x}(t_k^+)\\ \boldsymbol{\lambda}(t_k^+)\end{bmatrix} + \begin{bmatrix}-\boldsymbol{A}_{dk}^{-1}\boldsymbol{P}^{-1}(t_k^+)\\ -\boldsymbol{Q}_{dk}\boldsymbol{A}_{dk}^{-1}\boldsymbol{P}^{-1}(t_k^+)\end{bmatrix}\boldsymbol{h}(t_k^+) \quad (15)$$

where $\boldsymbol{Z}_k \triangleq \boldsymbol{P}^{-1}(t_k^+) + \boldsymbol{B}_{dk}\boldsymbol{R}_{dk}^{-1}\boldsymbol{B}_{dk}^T$. Rearranging (13) (with the definition of $\boldsymbol{Z}_k$ used) for $\boldsymbol{\lambda}(t_k^+)$ and substituting the result in (14) produce

$$\boldsymbol{\lambda}(t_k^-) = (\boldsymbol{Q}_{dk} + \boldsymbol{A}_{dk}^T\boldsymbol{Z}_k^{-1}\boldsymbol{A}_{dk})\boldsymbol{x}(t_k^-) + (\boldsymbol{A}_{dk}^T\boldsymbol{Z}_k^{-1}\boldsymbol{P}^{-1}(t_k^+))\boldsymbol{h}(t_k^+) \quad (16)$$

which is of the form $\boldsymbol{\lambda}(t_k^-) = \boldsymbol{P}(t_k^-)\boldsymbol{x}(t_k^-) + \boldsymbol{h}(t_k^-)$. After using the matrix inversion lemma for $\boldsymbol{Z}_k^{-1}$ and some further

manipulations, the following difference equations are obtained:

$$\boldsymbol{P}_k^- = \boldsymbol{Q}_{dk} + \boldsymbol{A}_{dk}^T \boldsymbol{P}_k^+ \boldsymbol{A}_{dk} - \boldsymbol{A}_{dk}^T \boldsymbol{P}_k^+ \boldsymbol{B}_{dk} \left(\boldsymbol{R}_{dk} + \boldsymbol{B}_{dk}^T \boldsymbol{P}_k^+ \boldsymbol{B}_{dk}\right)^{-1} \boldsymbol{B}_{dk}^T \boldsymbol{P}_k^+ \boldsymbol{A}_{dk} \tag{17a}$$

$$\boldsymbol{h}_k^- = \left(\boldsymbol{1} + \boldsymbol{A}_{dk}^T \boldsymbol{P}_k^+ \boldsymbol{B}_{dk} \boldsymbol{R}_{dk}^{-1} \boldsymbol{B}_{dk}^T \boldsymbol{A}_{dk}^{-T}\right)^{-1} \boldsymbol{A}_{dk}^T \boldsymbol{h}_k^+ \tag{17b}$$

where $\boldsymbol{P}_k^\pm \triangleq \boldsymbol{P}(t_k^\pm)$ and $\boldsymbol{h}_k^\pm \triangleq \boldsymbol{h}(t_k^\pm)$. The set of differential equations given by (12) is integrated backward in time, starting from the indicated terminal conditions. At each impulse time, a jump is induced in both solutions based on the set of difference equations in (17), and the computed $\boldsymbol{P}(t_k^-)$ and $\boldsymbol{h}(t_k^-)$ are used as new terminal conditions for (12) to be further integrated backward from t_k^- to t_{k-1}^+.

For the simulations, the nonlinear dynamics given by (1) are numerically integrated with user-specified initial conditions (ICs) for the states at $t = 0$. To determine the optimal magnetic dipole moments at $t \neq t_k$, the Riccati solution $\boldsymbol{P}(t)$ and the bias term $\boldsymbol{h}(t)$ are used with (9e). Similarly, the optimal thruster gains are computed at $t = t_k$ using the values of the two solutions immediately before each impulse, $\boldsymbol{P}(t_k^-)$ and $\boldsymbol{h}(t_k^-)$, with (9f). This procedure yields an optimal combination of control torques, produced by the following inputs, that accommodates the assumed disturbances:

$$\boldsymbol{m}^*(t) = -\boldsymbol{R}_c^{-1} \boldsymbol{B}_c^T(t) \left[\boldsymbol{P}(t)\boldsymbol{x}(t) + \boldsymbol{h}(t)\right] \tag{18a}$$

$$\boldsymbol{n}_k^* = -\boldsymbol{R}_{dk}^{-1} \boldsymbol{B}_{dk}^T \boldsymbol{A}_{dk}^{-T} \left[\left(\boldsymbol{P}_k^- - \boldsymbol{Q}_k\right)\boldsymbol{x}_k^- + \boldsymbol{h}_k^-\right]. \tag{18b}$$

IV. Optimal Impulse Times

The DA design approach proposed in Section III assumed that impulses are applied at some prescribed impulse times. This section investigates the necessary conditions for optimality of impulse times, such that the resulting cost function is smaller than that of any other set of impulse times, provided that the total number of impulses is known and fixed.

A. Summary of Previous Results

Variational principles similar to those presented in Section III are used in [16], while also allowing for variation in t_k, to derive the following transversality condition (Section IV-C and the Appendix also use an essentially identical approach, but for the special case of repeating impulses):

$$\Delta_k \triangleq \mathscr{H}_c\left(t_k^-\right) - \mathscr{H}_c\left(t_k^+\right) + \frac{\partial \mathscr{H}_d(t_k)}{\partial t_k} = 0 \tag{19}$$

which is necessary for each impulse time in order for the combination of t_ks to minimize J [given by (7)] over all possible impulse patterns (with known and fixed number of impulses). Even though the continuous Hamiltonian $\mathscr{H}_c(t)$ is defined differently in this brief, the above necessary condition remains the same, since its derivation is not affected by the inclusion of $\boldsymbol{d}(t)$ as in (8a).

Compared with [16], what does differ in this brief is what (19) translates to in the context of this particular DA attitude control problem. Section IV-B performs this study. In addition, Section IV-C shows that if the impulse pattern repeats in every orbit, one can conclude optimality by simply generating a grid in the first orbit and studying the sum of $\Delta_{k,i}$s computed at $t_k + iT$ [i.e., impulse times within the ith interval that correspond to the same $t_k \in [0, T)$].

B. Extension to Accommodate Disturbances

In this particular problem, $\boldsymbol{A}_{dk}$ and $\boldsymbol{B}_{dk}$ are constant, and assuming, for simplicity, that $\boldsymbol{Q}_{dk}$ and $\boldsymbol{R}_{dk}$ are constant too, the discrete Hamiltonian in (8b) becomes independent of t_k and $\partial \mathscr{H}_d(t_k)/\partial t_k = 0$. Consequently, the optimality condition in (19) becomes $\Delta_k = \mathscr{H}_c(t_k^-) - \mathscr{H}_c(t_k^+) = 0$.

Consider the continuous-time Hamiltonian in (8a) immediately before or after an impulse application time, i.e., at $t = t_k^\pm$

$$\left(\frac{1}{2} \underbrace{\begin{bmatrix} \boldsymbol{x}(t_k^\pm) \\ \boldsymbol{\lambda}(t_k^\pm) \end{bmatrix}}_{\boldsymbol{z}_k^\pm}^T \underbrace{\begin{bmatrix} \boldsymbol{Q}_c(t_k^\pm) & \boldsymbol{A}_c^T(t_k^\pm) \\ \boldsymbol{A}_c(t_k^\pm) & -\boldsymbol{B}_c(t_k^\pm)\boldsymbol{R}_c^{-1}(t_k^\pm)\boldsymbol{B}_c^T(t_k^\pm) \end{bmatrix}}_{\boldsymbol{H}_k^\pm} + \underbrace{\begin{bmatrix} \boldsymbol{0} \\ \boldsymbol{d}(t_k^\pm) \end{bmatrix}}_{\boldsymbol{I}_k^\pm}^T \right) \underbrace{\begin{bmatrix} \boldsymbol{x}(t_k^\pm) \\ \boldsymbol{\lambda}(t_k^\pm) \end{bmatrix}}_{\boldsymbol{z}_k^\pm} = \mathscr{H}_c(t_k^\pm) \tag{20}$$

where $\boldsymbol{H}_k^\pm$ (the same as that in [16]), $\boldsymbol{I}_k^\pm$, and $\boldsymbol{z}_k^\pm$ are defined for convenience. Solving (14) for $\boldsymbol{\lambda}(t_k^+)$, together with its substitution into the closed-loop discrete dynamics of $\boldsymbol{x}(t_k^+)$, yields the relationship $\boldsymbol{z}_k^+ = \boldsymbol{G}_k \boldsymbol{z}_k^-$ between the preimpulse and postimpulse states and costates, where $\boldsymbol{G}_k$ is defined as

$$\boldsymbol{G}_k \triangleq \begin{bmatrix} \boldsymbol{A}_{dk} + \boldsymbol{B}_{dk}\boldsymbol{R}_{dk}^{-1}\boldsymbol{B}_{dk}^T\boldsymbol{A}_{dk}^{-T}\boldsymbol{Q}_{dk} & -\boldsymbol{B}_{dk}\boldsymbol{R}_{dk}^{-1}\boldsymbol{B}_{dk}^T\boldsymbol{A}_{dk}^{-T} \\ -\boldsymbol{A}_{dk}^{-T}\boldsymbol{Q}_{dk} & \boldsymbol{A}_{dk}^{-T} \end{bmatrix}$$

and is identical to that in [16]. Substituting this relationship into (20) for the postimpulse Hamiltonian yields

$$\mathscr{H}_c(t_k^+) = \frac{1}{2} \boldsymbol{z}_k^{-T} \boldsymbol{G}_k^T \boldsymbol{H}_k^+ \boldsymbol{G}_k \boldsymbol{z}_k^- + \boldsymbol{I}_k^{+T} \boldsymbol{G}_k \boldsymbol{z}_k^-. \tag{21}$$

From Section III, we have $\boldsymbol{\lambda}(t_k^-) = \boldsymbol{P}(t_k^-)\boldsymbol{x}(t_k^-) + \boldsymbol{h}(t_k^-)$, using which the preimpulse state/costate vector is given by

$$\boldsymbol{z}_k^- = \begin{bmatrix} \boldsymbol{x}(t_k^-) \\ \boldsymbol{\lambda}(t_k^-) \end{bmatrix} = \underbrace{\begin{bmatrix} \boldsymbol{1} \\ \boldsymbol{P}(t_k^-) \end{bmatrix}}_{\boldsymbol{Y}_k^-} \boldsymbol{x}(t_k^-) + \underbrace{\begin{bmatrix} \boldsymbol{0} \\ \boldsymbol{h}(t_k^-) \end{bmatrix}}_{\boldsymbol{K}_k^-}. \tag{22}$$

Finally, substituting (22) into (21) and using (20) with $t = t_k^-$ for the preimpulse Hamiltonian produce

$$\mathscr{H}_c(t_k^+) = \frac{1}{2} \left[\boldsymbol{f}^T(\boldsymbol{x}_k^-)\boldsymbol{G}_k^T \boldsymbol{H}_k^+ \boldsymbol{G}_k + 2\boldsymbol{I}_k^{+T}\boldsymbol{G}_k\right] \boldsymbol{f}(\boldsymbol{x}_k^-) \tag{23a}$$

$$\mathscr{H}_c(t_k^-) = \frac{1}{2} \left[\boldsymbol{f}^T(\boldsymbol{x}_k^-)\boldsymbol{H}_k^- + 2\boldsymbol{I}_k^{-T}\right] \boldsymbol{f}(\boldsymbol{x}_k^-) \tag{23b}$$

where $\boldsymbol{f}(\boldsymbol{x}_k^-) \triangleq \boldsymbol{Y}_k^- \boldsymbol{x}(t_k^-) + \boldsymbol{K}_k^-$. Realizing that $\boldsymbol{I}_k^+ = \boldsymbol{I}_k^- = \boldsymbol{I}_k$ (since the disturbances are not affected by the impulses) and recalling that $\partial \mathscr{H}_d(t_k)/\partial t_k = 0$ owing to the constant

discrete-time penalty and state-space matrices assumption, subtracting (23a) from (23b) yields the following, upon expansion and simplification, for Δ_k of (19):

$$\Delta_k = \frac{1}{2}\Big[\boldsymbol{x}\big(t_k^-\big)^T \boldsymbol{M}_k \boldsymbol{x}\big(t_k^-\big) + \big(\boldsymbol{K}_k^{-T}\boldsymbol{N}_k + \boldsymbol{L}_k\big)\boldsymbol{K}_k^- + \big(\boldsymbol{K}_k^{-T}\big(\boldsymbol{N}_k + \boldsymbol{N}_k^T\big) + \boldsymbol{L}_k\big)\boldsymbol{Y}_k^- \boldsymbol{x}\big(t_k^-\big)\Big] = 0 \quad (24)$$

where $\boldsymbol{N}_k \triangleq \boldsymbol{H}_k^- - \boldsymbol{G}_k^T \boldsymbol{H}_k^+ \boldsymbol{G}_k$, $\boldsymbol{L}_k \triangleq 2\boldsymbol{I}_k^T(\boldsymbol{1} - \boldsymbol{G}_k)$, and $\boldsymbol{M}_k \triangleq \boldsymbol{Y}_k^{-T}\boldsymbol{N}_k\boldsymbol{Y}_k^-$. Comparing the result in (24) with that in [16, eq. (37)], one realizes that in addition to a quadratic term (which is the same for both relationships, as the $\boldsymbol{M}_k$s reduce to an identical definition if one lets $\boldsymbol{F}_k = \boldsymbol{0}$ in [16] considering $\partial \boldsymbol{A}_{dk}/\partial t_k = \boldsymbol{0}$ here), there now exists a linear term in $\boldsymbol{x}(t_k^-)$ as well as a bias term that is independent of $\boldsymbol{x}(t_k^-)$.

C. Extension to Multiple Orbits

Hitherto, we have the necessary conditions to check whether a set of impulses applied at t_k, $k \in \{1, \ldots, N-1\}$, with $N-1$ known and fixed, locally minimizes the cost function J associated with the DA hybrid attitude controller. These conditions are given as $\Delta_k = 0$ at each t_k, where the expressions used to compute Δ_k were presented in Section IV-B. Assume one were to use the brute force approach of discretizing the control interval, traversing all possible combinations of impulse times (for known and fixed $N-1$), and checking the necessary conditions at each t_k. This approach would be extremely computationally expensive for a multiorbit case in which each impulse time is allowed to vary independently of the others. In contrast, if one imposes the constraint that the impulse pattern in all orbits is identical (i.e., impulses are applied at the same times relative to the beginning of each orbit as those in the first orbit), the discretized grid that is traversed can be confined to the first orbit only. The aim of this section is to extend the optimality concepts presented so far to this special case.

Let the impulse application times over μ orbits, for $t \in [0, \mu T]$, be $t_k = t_\beta + iT$, where $t_\beta \in [0, T)$, $\beta \in \{1, \ldots, n-1\}$ refer to the $n-1$ impulse times *in the first orbit*. In addition, $i \in \{0, \ldots, \mu - 1\}$ indicates the ith orbit *after* the first one. With these definitions, the cost function is modified to incorporate the repeating pattern, and its differential is derived as described in the Appendix. Then, setting $dJ = 0$ for an extremum and arguing that the coefficients of all differentials must vanish, the following "extended" transversality conditions are obtained:

$$\Delta_\beta \triangleq \sum_{i=0}^{\mu-1}\left[\mathscr{H}_c\big(t_\beta^- + iT\big) - \mathscr{H}_c\big(t_\beta^+ + iT\big) + \frac{\partial \mathscr{H}_{d_{\beta,i}}}{\partial(t_\beta + iT)}\right] = 0 \quad (25)$$

where $\partial(\cdot)/\partial(t_\beta) = \partial(\cdot)/\partial(t_\beta + iT)$ is utilized. Note that $\Delta_\beta = \sum_{i=0}^{\mu-1}\Delta_{\beta,i} = 0$. This means that the same approach as that for a single-orbit case can be followed for multiple orbits with a periodic impulse pattern, but the extended optimality condition Δ_β corresponding to the $t_\beta \in [0, T)$ should be computed by summing (over all orbits within the control interval) the terms that would, in a more general case, represent Δ_k, given by (19) [or given by (24) specifically to this brief's DA problem], for distinct t_ks.

V. Numerical Examples

The effectiveness of the proposed DA hybrid LQR is studied via numerical integration of the nonlinear equations of motion given by (1) and (3). Prior to the simulation of the dynamics, $\boldsymbol{P}(t)$ and $\boldsymbol{h}(t)$ are determined by integrating (12) backward from the terminal time using a fourth-order Runge–Kutta scheme, inducing jumps in the solutions using (17) at each impulse time, and using $\boldsymbol{P}(t_k^-)$ and $\boldsymbol{h}(t_k^-)$ as the new terminal conditions for backward integration until time 0 is reached. Then, during the forward nonlinear simulation via RK4, the control torques are computed using (18) and added to the estimated disturbance torques at each time.

A circular near-polar Keplerian orbit with an altitude of 450 km and orbital parameters $\{e, i, \Omega, \omega, t_0\} = \{0, 87°, 0\text{ rad}, 0\text{ rad}, 0\text{ s}\}$ (representing eccentricity, inclination, right ascension of ascending node, argument of periapsis, and time of perigee passage, respectively) is assumed. Residual dipole moments resulting from the on-board electronics are assumed to be $\boldsymbol{m}_{\text{dist}} = [0.01\ \ 0.01\ \ 0.01]^T$ A $\cdot$ m^2. The spacecraft's moment of inertia is set to $\boldsymbol{I} = \text{diag}\{27, 17, 25\}$ kg $\cdot$ m^2.

The penalty matrices used in (7) are taken as constant. To reduce the size of the design space and for simplicity, these matrices are set to $\boldsymbol{Q}_c = \text{blockdiag}\{q_c \cdot \boldsymbol{1}_{3\times3}, q_c \cdot \boldsymbol{I}\}$ and $\boldsymbol{Q}_d = \text{blockdiag}\{q_d \cdot \boldsymbol{1}_{3\times3}, q_d \cdot \boldsymbol{I}\}$ for the state penalties, and $\boldsymbol{R}_c = r_c \cdot \boldsymbol{1}_{3\times3}$ and $\boldsymbol{R}_d = r_d \cdot \boldsymbol{1}_{3\times3}$ for the control penalties. The scalar parameters are then tuned to produce satisfactory performance by balancing the penalty on the states compared with that on the control, as well as by balancing the penalty on continuous dynamics/control compared with that on the discrete dynamics/control. For the numerical examples presented here, these parameters are set to $r_c = 3 \times 10^5$, $q_c = 10^8$, $r_d = 10^{13}$, and $q_d = 10^{10}$. The terminal penalty is set to $\boldsymbol{S} = \boldsymbol{P}(t_f) = \boldsymbol{0}$.

A. Extended Optimality Conditions and Multiple Orbits

To validate the optimal impulse timing conditions for multiple orbits and with disturbance accommodation, given by (24) and (25), a 100-point grid is defined on $[0, T)$ for selecting a single-impulse application time. A brute force approach is used to compute the cost function, J [given by (7)]: the grid is traversed with $t_1 \in \{0, 0.01, \ldots, 0.99\} \times T$, while the simulation is run over five orbital periods with repeating patterns of impulses applied at $t_k = t_{1,i} = t_1 + iT$, $i \in \{0, \ldots, 4\}$. In the meantime, the extended optimality condition of (25), $\Delta_1 = \sum_{i=0}^{4}\Delta_{1,i}$, is computed for each choice of t_1 by summing over the $\Delta_{1,i}$s [given by (24) that accounts for the disturbances] evaluated at each impulse time, $t_k = t_{1,i}$, with $i \in \{0, \ldots 4\}$. Since the theory is derived using a linearized model, the nonlinear simulation is run with zero ICs ($\boldsymbol{\epsilon}_0 = \boldsymbol{0}$, $\eta_0 = 1$, and $\boldsymbol{\omega}_0 = \boldsymbol{0}$ rad/s) to ensure that the angles and rates are small enough for the linearity assumption to remain valid.

The results of this simulation are presented in Fig. 1. The total cost J computed over five orbits is shown in Fig. 1(a). The $\Delta_{1,i}$s computed separately at each orbit $i \in \{0, \ldots, 4\}$ are shown in Fig. 1(b), while their sum is depicted in Fig. 1(c). Interestingly, the global minimum of J occurs at the boundary,

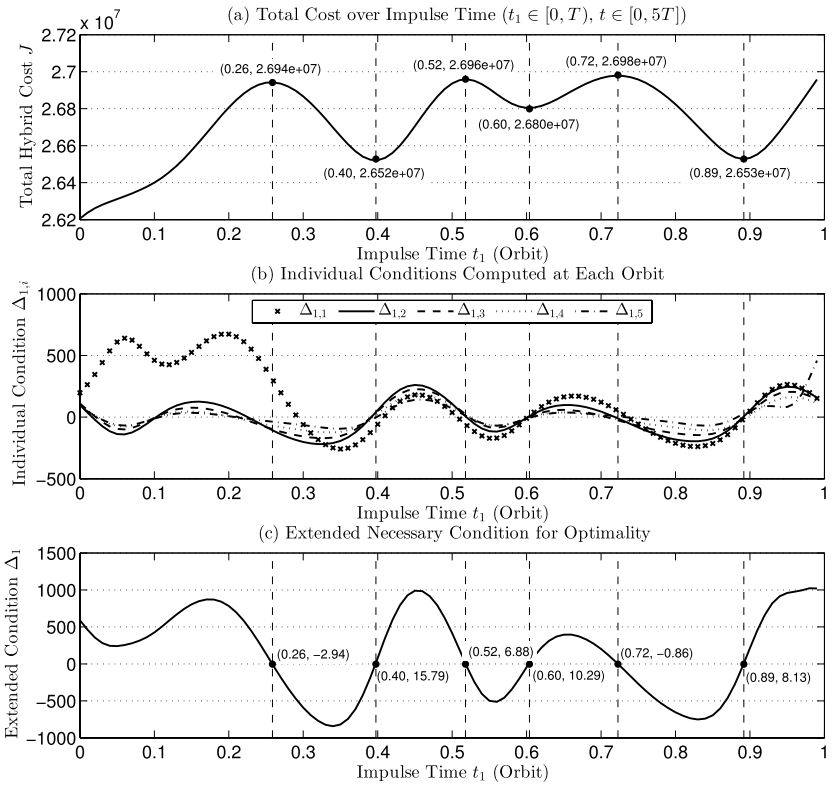

Fig. 1. Optimal 1-impulse timing with zero ICs, $t_1 \in \{0, 0.01, \ldots, 0.99\} \times T$ and $t \in [0, 5T]$. ($r_c = 3 \times 10^5$, $q_c = 10^8$, $r_d = 10^{13}$, and $q_d = 10^{10}$) (a) Total cost computed over five orbits. (b) Individual conditions $\Delta_{1,i}$ computed at the ith orbit. (c) Extended optimality condition $\Delta_1 = \sum_{i=0}^{4} \Delta_{1,i}$.

$t_1 = 0$, which means that an impulse right at the beginning results in the smallest cost. There is no apparent correspondence between Fig. 1(a) and (b), as expected, whereas the local extrema of J in Fig. 1(a) exactly correspond to the zeros of Δ_1 in Fig. 1(c), confirming the validity of the extended optimality condition theory presented in Section IV-C. Also validated is the extension to accommodate disturbances (presented in Section IV-B), because $\Delta_{1,i}$s accumulated to yield Δ_1 are computed using (24), which includes the disturbance effects.

Although this simulation case and, in general, that presented in Section IV-C are a special case with periodic impulses, significant reduction in computational effort ensues from this constraint: the only degree of freedom for the impulse time(s) is in the first orbit. If one were to use the original theory of [16] to find the optimal combination of five impulse times over five orbits with no restriction on their relative timing (except that they should occur in different orbits), the same fine grid of $0.01T$ mesh size would require 100^5 computations owing to the five degrees of freedom for t_k, in contrast to only 100 needed in this restricted (yet still useful) case of T-periodic impulses.

B. Performance of DA Hybrid Magnetic LQR

In this section, the disturbance rejection performance of the DA hybrid magnetic LQR is studied, in particular in comparison with that of the regular (nonaccommodating) hybrid LQR. The same penalty matrices and ICs as those in Section V-A ($\boldsymbol{\epsilon}_0 = \mathbf{0}$, $\eta_0 = 1$, and $\boldsymbol{\omega}_0 = \mathbf{0}$ rad/s) are used. Based on Fig. 1, which suggests that the best time to apply a thrust in a single-impulse case is at the beginning, $t_1 = 0$ is chosen here for both regular and DA hybrid LQRs. Because there is no transient behavior resulting from nonzero ICs, these results can be viewed as the controllers' steady-state performance. To assess the robustness of the proposed DA LQR with respect to accuracy of the assumed disturbances, the controller is designed using $\boldsymbol{I} = \text{diag}\{25, 15, 25\}$ kg $\cdot$ m^2 and $\boldsymbol{m}_{\text{dist}} = [0.009\ 0.009\ 0.009]^T$ A $\cdot$ m^2, reflecting about 10% error compared with the truth model.

Shown in Fig. 2 are the nonlinear simulation results using zero ICs. Although the second components are not affected, improvements are seen in the steady-state control of the other components. The improvements become much more pronounced (with significantly better control of the two components) when the design and truth models of the disturbances match, but these results are not included.

Table I lists the values of some parameters defined to enable quantitative studies on the controllers' performance. The controllers tested are solely magnetic LQR with no impulses, hybrid LQR with $t_1 = 0$, and DA hybrid LQR with $t_1 = 0$. In addition to the total cost, the performance parameters include the electrical energy consumption, $E = 3R/(c^2A^2) \int_0^T \boldsymbol{m}^T \boldsymbol{m} dt$, assuming three mutually perpendicular magnetic torque coils with resistance $R = 100\ \Omega$, $c = 400$ turns, and diameter $d = 10$ mm based on some representative missions presented in [18]. Also included are some rms-like norms defined as $\|\boldsymbol{\tau}\|_{5T} \triangleq ((\int_0^{5T} \boldsymbol{\tau}_{\text{mag}}^T \boldsymbol{\tau}_{\text{mag}} dt)/(5T))^{1/2}$

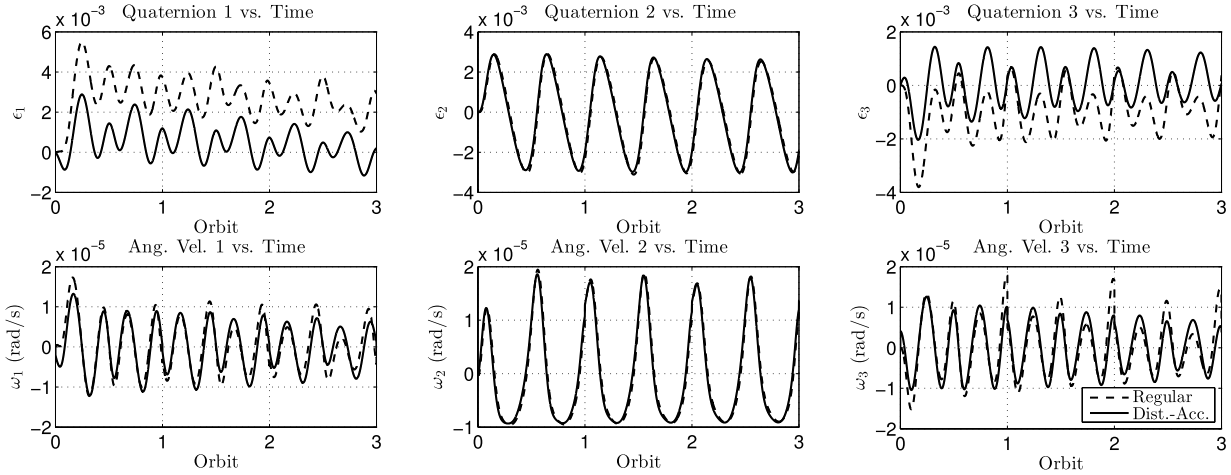

Fig. 2. Quaternions and angular velocity: regular (dashed line) versus DA (solid line) hybrid magnetic LQR ($r_c = 3 \times 10^5$, $q_c = 10^8$, $r_d = 10^{13}$, and $q_d = 10^{10}$).

TABLE I

PERFORMANCE OF REGULAR MAGNETIC, REGULAR LQR, AND DA LQR OVER $5T$ ($r_c = 3 \times 10^5$ AND $q_c = 10^8$, AND FOR THE HYBRID CONTROLLERS ALSO, $r_d = 10^{13}$ AND $q_d = 10^{10}$)

Param.	Magnetic	Regular	Dist.-Acc.	Unit
J_{5T}	9.57×10^{7}	9.63×10^{7}	5.97×10^{7}	-
E_{5T}	6.03×10^{1}	6.04×10^{1}	5.94×10^{1}	MJ
$\|\|\boldsymbol{\tau}\|\|_{5T}$	3.06×10^{-6}	3.06×10^{-6}	3.05×10^{-6}	N·m
$\|\|\boldsymbol{v}\|\|_{5T}$	0	1.06×10^{-5}	3.62×10^{-6}	N·m
$\|\|\boldsymbol{\omega}\|\|_{5T}$	1.23×10^{-5}	1.23×10^{-5}	1.17×10^{-5}	rad/s
$\|\|\phi\|\|_{5T}$	6.86×10^{-3}	6.74×10^{-3}	4.61×10^{-3}	rad

for magnetic torques, $||\boldsymbol{v}||_{5T} \triangleq ((\int_0^{5T} \boldsymbol{\tau}_{\text{imp}}^T \boldsymbol{\tau}_{\text{imp}} dt)/(5T))^{1/2}$ for impulsive torques, $||\boldsymbol{\omega}||_{5T} \triangleq ((\int_0^{5T} \boldsymbol{\omega}^T \boldsymbol{\omega} dt)/(5T))^{1/2}$ for angular velocity, and $||\phi||_{5T} \triangleq ((\int_0^{5T} \phi^2 dt)/(5T))^{1/2}$ for rotation angle (from Euler's axis/angle parameters). For $||\boldsymbol{v}||_{5T}$, a finite-width approximation of Dirac delta is used, and to compute ϕ, $\cos(\phi) = (\text{trace}\{\boldsymbol{C}_{\text{BG}}\} - 1)/2$ is used.

The values in Table I highlight the superiority of the DA hybrid magnetic controller in disturbance rejection for this choice of penalties. Although the regular hybrid LQR was shown in [12] to improve the transient for the same set of penalties as that of this brief, based on Table I, it seems to offer little improvement (if any) in steady-state performance compared with a solely magnetic controller. On the other hand, the DA hybrid LQR reduces all parameters (including a 38% reduction in J) thanks to the disturbance awareness inherent in its design.

VI. CONCLUSION

Modifications have been suggested to the hybrid (continuous/impulsive) attitude control scheme proposed in [12] in order to accommodate disturbance torques resulting from gravity gradient and residual magnetic dipole moments, both of which can be estimated *a priori*. Similar to the Riccati solution, continuous- and discrete-time equations have been derived to describe the evolution of the disturbance-rejecting bias term over time and the optimal control inputs have been modified accordingly. The simulation results with zero ICs have been presented that suggest steady-state performance improvement as a result of disturbance accommodation.

In addition, the implications of the necessary conditions for optimality of impulse times presented in [16] have been studied in the context of the DA attitude control problem of this brief. The conditions have been shown to require extra terms to be added to the familiar quadratic form discussed in [16] in order to account for the disturbances. It has also been shown, in the special case of repeating impulse patterns, that the extended necessary condition (with degrees of freedom only in the first orbit) would simply involve the summation (over all orbits in the control interval) of the terms that would originally represent the optimality conditions computed at distinct impulse times. Multiorbit simulation results with zero ICs validated both extensions to the optimality conditions.

APPENDIX
DIFFERENTIAL OF COST FUNCTION FOR MULTIPLE ORBITS

This section presents a variational approach to derive the differential of the cost function associated with repeating impulse patterns over μ orbits, $t \in [0, \mu T]$. Let $t_\beta \in [0, T)$, $\beta \in \{1, \ldots, n-1\}$ be the $n-1$ impulse times *in the first orbit*, such that $t_k = t_\beta + iT$, where $i \in \{0, \ldots, \mu - 1\}$ indicates the ith orbit *after* the first one. Let $t_0^+ = 0$ and $t_n^- = T$. The hybrid performance index J [given by (7)] can be modified to reflect the imposed restriction on a periodic impulse pattern and that $t_f = \mu T$, and can be rewritten using (8) as follows:

$$\begin{aligned} J = J_f + J_c + J_d \triangleq \frac{1}{2}\boldsymbol{x}^T(\mu T)\boldsymbol{S}\boldsymbol{x}(\mu T) \\ + \sum_{i=0}^{\mu-1}\sum_{\beta=0}^{n-1}\int_{t_\beta^+ + iT}^{t_{\beta+1}^- + iT} [\mathscr{H}_c(t) - \boldsymbol{\lambda}^T(t)\dot{\boldsymbol{x}}(t)]dt \\ + \sum_{i=0}^{\mu-1}\sum_{\beta=1}^{n-1}\left[\mathscr{H}_d(t_\beta + iT) - \boldsymbol{v}_{k,i}^T\boldsymbol{x}\left(t_\beta^+ + iT\right)\right] \quad (26) \end{aligned}$$

where J_f, J_c, and J_d represent the terminal, continuous-time, and discrete-time costs, respectively. We now take the

differential of J following the same approach as that in [16]:

$$dJ_f = \boldsymbol{x}^T(\mu T)\boldsymbol{S}d\boldsymbol{x}(\mu T) \tag{27a}$$

$$dJ_c = \sum_{i=0}^{\mu-1}\sum_{\beta=0}^{n-1}\delta\left\{\int_{t_\beta^+ + iT}^{t_{\beta+1}^- + iT}[\mathscr{H}_c - \boldsymbol{\lambda}^T\dot{\boldsymbol{x}}]dt\right\} + \sum_{\beta=0}^{n-1}\frac{d}{dt_\beta}\left\{\sum_{j=0}^{\mu-1}\sum_{\iota=0}^{n-1}\int_{t_\iota^+ + jT}^{t_{\iota+1}^- + jT}[\mathscr{H}_c - \boldsymbol{\lambda}^T\dot{\boldsymbol{x}}]dt\right\}dt_\beta \tag{27b}$$

$$dJ_d = \sum_{i=0}^{\mu-1}\sum_{\beta=1}^{n-1}\left[\frac{\partial\mathscr{H}_{d_{\beta,i}}}{\partial\boldsymbol{x}_{\beta,i}^-}^T d\boldsymbol{x}_{\beta,i}^- + \frac{\partial\mathscr{H}_{d_{\beta,i}}}{\partial\boldsymbol{v}_{\beta,i}}^T d\boldsymbol{v}_{\beta,i} + \frac{\partial\mathscr{H}_{d_{\beta,i}}}{\partial t_\beta}dt_\beta - \boldsymbol{v}_{\beta,i}^T d\boldsymbol{x}_{\beta,i}^+\right] \tag{27c}$$

where the shortened subscript "β, i" denotes "$\beta + i(n-1)$," $\boldsymbol{x}_{\beta,i}^- \triangleq \boldsymbol{x}(t_\beta^- + iT)$, and $\mathscr{H}_{d_{\beta,i}} \triangleq \mathscr{H}_d(t_\beta + iT)$. In addition, $\partial(\cdot)/\partial(t_\beta + iT) = \partial(\cdot)/\partial(t_\beta)$ is used, since all the impulses $t_\beta + iT$ corresponding to t_β from the first orbit are dictated by t_β. Note that (27b) is written considering the noncontemporaneous differential, analogously to how the state's differential must be computed for any t_β [16]

$$d\boldsymbol{x}(t_k^\pm) = \delta\boldsymbol{x}(t_k^\pm) + \dot{\boldsymbol{x}}(t_k^\pm)d(t_k). \tag{28}$$

Now, taking the variation in the first part of (27b) inside the integral and noting that $\mathscr{H}_c$ is not directly a function of t_k

$$\sum_{i=0}^{\mu-1}\sum_{\beta=0}^{n-1}\delta\left\{\int_{t_\beta^+ + iT}^{t_{\beta+1}^- + iT}[\mathscr{H}_c(t) - \boldsymbol{\lambda}^T(t)\dot{\boldsymbol{x}}(t)]dt\right\} = \sum_{i=0}^{\mu-1}\sum_{\beta=0}^{n-1}\left\{\int_{t_\beta^+ + iT}^{t_{\beta+1}^- + iT}\left[\frac{\partial\mathscr{H}_c(t)}{\partial\boldsymbol{x}(t)}^T\delta\boldsymbol{x}(t) + \frac{\partial\mathscr{H}_c(t)}{\partial\boldsymbol{u}(t)}^T\delta\boldsymbol{u}(t) + \dot{\boldsymbol{\lambda}}^T(t)\delta\boldsymbol{x}(t)\right]dt - \boldsymbol{\lambda}^T(t)\delta\boldsymbol{x}(t)\Big|_{t_\beta^+ + iT}^{t_{\beta+1}^- + iT}\right\} \tag{29}$$

where integration by parts is performed. While traversing all orbits by increasing i from 0 to $\mu - 1$, the last term of $\sum_{\beta=0}^{n-1} -\boldsymbol{\lambda}^T\delta\boldsymbol{x}|_{t_\beta^+ + iT}^{t_{\beta+1}^- + iT}$ for the ith orbit will cancel the first term of the expression for the $(i+1)$th orbit. Thus, we have

$$\sum_{i=0}^{\mu-1}\sum_{\beta=0}^{n-1} -\boldsymbol{\lambda}^T(t)\delta\boldsymbol{x}(t)\Big|_{t_\beta^+ + iT}^{t_{\beta+1}^- + iT} = -\boldsymbol{\lambda}^T(\mu T)\cancel{\delta\boldsymbol{x}(\mu T)}^{d\boldsymbol{x}(\mu T)} + \cancel{\boldsymbol{\lambda}^T(0)\delta\boldsymbol{x}(0)}^{0} + \left(\sum_{i=0}^{\mu-1}\sum_{\beta=1}^{n-1}\boldsymbol{\lambda}^T(t)\delta\boldsymbol{x}(t)\Big|_{t_\beta^- + iT}^{t_\beta^+ + iT}\right) \tag{30}$$

where $\delta\boldsymbol{x}(t_0^+) = \delta\boldsymbol{x}(0) = \boldsymbol{0}$ (dictated by the ICs) and $t_n^- + (\mu-1)T = \mu T = t_f$ are evoked. In addition, (28) is used with $dt_f = 0$ to equate the terminal state's variation and differential.

Using Leibniz's integration rule on the second part of (27b)

$$\sum_{\beta=0}^{n-1}\frac{d}{dt_\beta}\left\{\sum_{j=0}^{\mu-1}\sum_{\iota=0}^{n-1}\int_{t_\iota^+ + jT}^{t_{\iota+1}^- + jT}\mathscr{H}_c - \boldsymbol{\lambda}^T\dot{\boldsymbol{x}}\,dt\right\}dt_\beta = \sum_{\beta=0}^{n-1}\left\{\sum_{j=0}^{\mu-1}\left(\mathscr{H}_c - \boldsymbol{\lambda}^T\dot{\boldsymbol{x}}\right)\Big|_{t_\beta^- + jT} - \left(\mathscr{H}_c - \boldsymbol{\lambda}^T\dot{\boldsymbol{x}}\right)\Big|_{t_\beta^+ + jT}\right\}dt_\beta \tag{31}$$

since $d(t_{\iota+1}^- + jT)/dt_\beta = 1$ only when $\iota + 1 = \beta$ and it is 0 otherwise, while $d(t_\iota^+ + jT)/dt_\beta = 1$ only when $\iota = \beta$ and it is 0 otherwise. Furthermore, taking into account that $d(t_0 + iT) = d(iT) = 0$ and $d(t_\beta^\pm + iT) = dt_\beta$ for any impulse time, the right-hand side of (31) can be rewritten as

$$\sum_{i=0}^{\mu-1}\sum_{\beta=1}^{n-1} -\mathscr{H}_c\Big|_{t_\beta^- + iT}^{t_\beta^+ + iT}dt_\beta + \sum_{i=0}^{\mu-1}\sum_{\beta=1}^{n-1}\left(\boldsymbol{\lambda}^T\dot{\boldsymbol{x}}dt\right)\Big|_{t_\beta^- + iT}^{t_\beta^+ + iT}. \tag{32}$$

Substituting (30) into (29) and adding the result to (31) yields an alternative form for dJ_c given by (27b), part of which can be further simplified using (28). Finally, passing this simplified form of dJ_c to (27a) and (27c) and collecting the like terms yield the following for dJ:

$$\begin{aligned} dJ = &\sum_{i=0}^{\mu-1}\sum_{\beta=0}^{n-1}\int_{t_\beta^+ + iT}^{t_{\beta+1}^- + iT}\left(\frac{\partial\mathscr{H}_c}{\partial\boldsymbol{x}}^T + \dot{\boldsymbol{\lambda}}^T\right)\delta\boldsymbol{x} + \frac{\partial\mathscr{H}_c}{\partial\boldsymbol{u}}^T\delta\boldsymbol{u}dt \\ &+\sum_{\beta=1}^{n-1}\sum_{i=0}^{\mu-1}\left[\left(\frac{\partial\mathscr{H}_{d_{\beta,i}}}{\partial\boldsymbol{x}_{\beta,i}^-}^T - \boldsymbol{\lambda}^T\left(t_\beta^- + iT\right)\right)d\boldsymbol{x}_{\beta,i}^- \right. \\ &+\left(\boldsymbol{\lambda}^T\left(t_\beta^+ + iT\right) - \boldsymbol{v}_{k,i}^T\right)d\boldsymbol{x}_{\beta,i}^+ + \frac{\partial\mathscr{H}_{d_{\beta,i}}}{\partial\boldsymbol{v}_{\beta,i}}^T d\boldsymbol{v}_{\beta,i} \\ &\left.+\left(\mathscr{H}_c\left(t_\beta^- + iT\right) - \mathscr{H}_c\left(t_\beta^+ + iT\right) + \frac{\partial\mathscr{H}_{d_{\beta,i}}}{\partial t_\beta}\right)dt_\beta\right] \\ &+(\boldsymbol{x}^T(\mu T)\boldsymbol{S} - \boldsymbol{\lambda}^T(\mu T))d\boldsymbol{x}(\mu T). \end{aligned} \tag{33}$$

The result is, thus, similar to [16, eq. (11)], but with $t_k = t_\beta + iT$ and an additional summation over all orbits.

REFERENCES

[1] E. Silani and M. Lovera, "Magnetic spacecraft attitude control: A survey and some new results," *Control Eng. Pract.*, vol. 13, no. 3, pp. 357–371, Mar. 2005.

[2] M. Lovera and A. Astolfi, "Spacecraft attitude control using magnetic actuators," *Automatica*, vol. 40, no. 8, pp. 1405–1414, Aug. 2004.

[3] R. Wiśniewski, "Linear time-varying approach to satellite attitude control using only electromagnetic actuation," *J. Guid., Control, Dyn.*, vol. 23, no. 4, pp. 640–647, Jul./Aug. 2000.

[4] R. Wiśniewski and M. Blanke, "Fully magnetic attitude control for spacecraft subject to gravity gradient," *Automatica*, vol. 35, no. 7, pp. 1201–1214, Jul. 1999.

[5] C. J. Damaren, "Comments on 'fully magnetic attitude control for spacecraft subject to gravity gradient,'" *Automatica*, vol. 38, no. 12, p. 2189, Dec. 2002.

[6] M. L. Psiaki, "Magnetic torquer attitude control via asymptotic periodic linear quadratic regulation," *J. Guid., Control, Dyn.*, vol. 24, no. 2, pp. 386–394, Mar./Apr. 2001.

[7] M. Lovera, E. De Marchi, and S. Bittanti, "Periodic attitude control techniques for small satellites with magnetic actuators," *IEEE Trans. Control Syst. Technol.*, vol. 10, no. 1, pp. 90–95, Jan. 2002.

[8] M. Lovera and A. Astolfi, "Global magnetic attitude control of inertially pointing spacecraft," *J. Guid., Control, Dyn.*, vol. 28, no. 5, pp. 1065–1072, Sep./Oct. 2005.

[9] C. J. Damaren, "Hybrid magnetic attitude control gain selection," *Proc. Inst. Mech. Eng. G, J. Aerosp. Eng.*, vol. 223, no. 8, pp. 1041–1047, Aug. 2009.

[10] J. R. Forbes and C. J. Damaren, "Linear time-varying passivity-based attitude control employing magnetic and mechanical actuation," *J. Guid., Control, Dyn.*, vol. 34, no. 5, pp. 1363–1372, Sep./Oct. 2011.

[11] T. Pulecchi and M. Lovera, "Attitude control of spacecraft with partially magnetic actuation," *IFAC Proc. Volumes*, vol. 40, no. 7, pp. 609–614, 2007.

[12] B. Vatankhahghadim and C. J. Damaren, "Optimal combination of magnetic attitude control with impulsive thrusting," *J. Guid., Control, Dyn.*, to be published. [Online]. Available: http://arc.aiaa.org/doi/abs/10.2514/1.G001664, doi: 10.2514/1.G001664.

[13] L. A. Sobiesiak and C. J. Damaren, "Optimal continuous/impulsive control for Lorentz-augmented spacecraft formations," *J. Guid., Control, Dyn.*, vol. 38, no. 1, pp. 151–157, Jan. 2015.

[14] H. M. Chun, J. D. Turner, and J.-N. Juang, "Disturbance-accommodating tracking maneuvers of flexible spacecraft," *J. Astron. Sci.*, vol. 33, no. 2, pp. 147–161, Apr./Jun. 1985.

[15] M. E. Pittelkau, "Optimal periodic control for spacecraft pointing and attitude determination," *J. Guid., Control, Dyn.*, vol. 16, no. 6, pp. 1078–1084, Nov./Dec. 1993.

[16] L. A. Sobiesiak and C. J. Damaren, "Lorentz-augmented spacecraft formation reconfiguration," *IEEE Trans. Control Syst. Technol.*, vol. 24, no. 2, pp. 514–524, Mar. 2016.

[17] P. C. Hughes, *Spacecraft Attitude Dynamics*. New York, NY, USA: Wiley, 1986.

[18] J. R. Wertz, Ed., *Spacecraft Attitude Determination and Control*. Dordrecht, The Netherlands: Reidel, 1978.

[19] M. Athans and P. L. Falb, *Optimal Control: An Introduction to the Theory and Its Applications*. New York, NY, USA: McGraw-Hill, 1966.